Second-forbidden nonunique β^- decays of ^{24}Na and ^{36}Cl assessed by the nuclear shell model

Anil Kumar,[1,*] Praveen C. Srivastava,[1,†] Joel Kostensalo,[2,‡] and Jouni Suhonen[2,§]
[1]*Department of Physics, Indian Institute of Technology Roorkee, Roorkee 247 667, India*
[2]*University of Jyvaskyla, Department of Physics, P.O. Box 35 (YFL), FI-40014, University of Jyvaskyla, Finland*

(Received 15 April 2020; accepted 22 May 2020; published 8 June 2020)

We have performed a systematic study of the log ft values, shape factors, and electron spectra for the second-forbidden nonunique β^- decays of ^{24}Na$(4^+) \rightarrow ^{24}$Mg(2^+) and ^{36}Cl$(2^+) \rightarrow ^{36}$Ar(0^+) transitions under the framework of the nuclear shell model. We have performed the shell model calculations in the *sd* model space, using more recent microscopic effective interactions such as Daejeon16, chiral N3LO, and JISP16. These interactions are derived from the no-core shell model wave functions using Okubo-Lee-Suzuki transformation. For comparison, we have also shown the results obtain from the phenomenological USDB interaction. To test the predictive power of these interactions first we have computed low-lying energy spectra of parent and daughter nuclei involved in these transitions. The computed results for energy spectra, nuclear matrix elements, log ft values, shape factors, electron spectra, and decomposition of the integrated shape factor are reported and compare with the available experimental data.

DOI: 10.1103/PhysRevC.101.064304

I. INTRODUCTION

β decay plays an important role in astrophysics, e.g., for the *r* process [1]. In the nuclear chart, there are selected candidates for double-β decays, but on the other hand there are several potential candidates known for forbidden β decay. Out of these, only around 27 possible candidates of second-forbidden nonunique β decay are observed, as reported in Ref. [2]. Recently, a new candidate was observed corresponding to second-forbidden nonunique decay of ^{20}F$(2^+) \rightarrow ^{20}$Ne(0^+) from ground-state-to-ground-state transition [3–5]. This study could change our understanding of the fate of intermediate-mass stars. A comprehensive review on the theoretical and experimental status of single- and double-β decay was recently reported in Ref. [6].

In β decay, based on the value of angular momentum (l) we can characterize any decay as allowed or forbidden. The $l = 0$ decays are called "allowed" while the $l > 0$ decays are called "forbidden." Further, we can divide decays as forbidden unique (FU) and forbidden nonunique (FNU). In the case of FU, the total angular momentum $K = l + 1$, whereas in FNU decay $K = l$. The β decay half-life of the fourth-forbidden nonunique decay of ^{50}V using the nuclear shell model is reported in Ref. [7]. The fourth-forbidden nonunique ground-state-to-ground-state β^- decay branches of ^{113}Cd and ^{115}In using the microscopic quasiparticle-phonon model and the nuclear shell model are reported in Refs. [8,9]. Also in these references the half-life method [8] and spectrum-shape method (SSM) [9] are reported to extract the value of axial-vector coupling constant g_A.

Studies of forbidden β decay using the nuclear shell model with phenomenological interactions are available in the literature. With the recent progress in the *ab initio* approaches for nuclear structure study, it is highly desirable to see how these interactions are able to predict nuclear observables such as forbidden β decay. Recently, shell model results for allowed β decay properties of *sd*, *fp*, and *fpg* shell nuclei were reported by us in Refs. [10–13].

In the present work, our aim is to study second-forbidden nonunique β^- transitions of ^{24}Na$(4^+) \rightarrow ^{24}$Mg(2^+) and ^{36}Cl$(2^+) \rightarrow ^{36}$Ar(0^+) using *ab initio* interactions. β-decay transitions in these nuclei have been calculated and compared with the available experimental data to test the quality of the *ab initio* interaction wave functions. A theoretical attempt has been made in the past to calculate the β decay transition observable of ^{36}Cl [14]. However, no theoretical estimate is found in the literature for the β decay of ^{24}Na and also no experimental shape factors and electron spectra are found in the literature. Thus, our theoretical predictions for the β decay of ^{24}Na are useful for the future experiments. In this work, we have computed the log ft values, shape factors, and electron spectra of these branches. We have constrained the relativistic nuclear matrix element based on conserved vector current (CVC) theory and tested the role of this matrix element in the shape factors and electron spectra. In order to test our computed wave functions, first we computed the low-lying energy spectra of ^{24}Na, ^{24}Mg, ^{36}Cl, and ^{36}Ar and compared them with the available experimental energy spectra [15].

This article is organized as follows. In Sec. II we give a short overview of the theoretical formalism for the β^- decay and details about microscopic effective interactions. Results and discussions corresponding to low-lying energy spectra,

*akumar5@ph.iitr.ac.in
†Corresponding author: praveen.srivastava@ph.iitr.ac.in
‡joel.j.kostensalo@student.jyu.fi
§jouni.t.suhonen@jyu.fi

nuclear matrix elements, log ft values, shape factors, electron spectra, and decomposition of the integrated shape factors are reported in Sec. III. Finally, in Sec. IV we draw the conclusions.

II. THEORETICAL FORMALISM

In Sec. II A we discuss the theory of forbidden β^- decay and the shape of the electron spectra. Section II B give the details about the valence space and microscopic effective interactions used in the present work.

A. β decay theory

The full details of formalism for both allowed and forbidden types of the β decay are available in the literature by Behrens and Bühring [16] (see also Ref. [17]). The generalized framework of the forbidden nonunique β decay theory is available in Refs. [9,18,19]. When the β decay process is described as a pointlike interaction vertex with an effective Fermi coupling constant $G_{\rm F}$, the probability of the electron emission in the kinetic energy interval W_e and $W_e + dW_e$ is expressed as

$$P(W_e)dW_e = \frac{G_{\rm F}^2}{(\hbar c)^6}\frac{1}{2\pi^3\hbar}C(W_e) \times p_e c W_e (W_0 - W_e)^2 F_0(Z, W_e) dW_e. \quad (1)$$

Where the $C(W_e)$ is the shape factor containing the nuclear structure information, and W_0 is the endpoint energy of the β spectrum. The factor $F_0(Z, W_e)$ is the Fermi function, which takes into account Coulombic interaction between the daughter nucleus and β particle, and Z is the proton number of the final nucleus. Furthermore, p_e and W_e are the momentum and energy of the emitted electron, respectively.

The partial half-life of the β decay is expressed as

$$t_{1/2} = \frac{\ln(2)}{\int_{m_e c^2}^{W_0} P(W_e)dW_e}, \quad (2)$$

where m_e is the mass of the electron. For convenience, Eq. (2) can be expressed in the form

$$t_{1/2} = \frac{\kappa}{\tilde{C}}, \quad (3)$$

where $\tilde{C}$ is the unitless integrated shape factor, and the constant κ has the value

$$\kappa = \frac{2\pi^3\hbar^7 \ln(2)}{m_e^5 c^4 (G_{\rm F}\cos\theta_{\rm C})^2} = 6147 \text{ s}, \quad (4)$$

where θ_C is the Cabibbo angle and the usual dimensionless kinematics quantities are defined as $w_0 = W_0/m_e c^2$, $w_e = W_e/m_e c^2$, and $p = p_e c/m_e c^2 = \sqrt{(w_e^2 - 1)}$. Then the dimensionless integrated shape factor $\tilde{C}$ can be expressed as

$$\tilde{C} = \int_1^{w_0} C(w_e) p w_e (w_0 - w_e)^2 F_0(Z, w_e) dw_e. \quad (5)$$

The comparative half-life, or the ft value, is obtained by multiplying the partial half-life with the following dimensionless integrated Fermi function:

$$f_0 = \int_1^{w_0} p w_e (w_0 - w_e)^2 F_0(Z, w_e) dw_e, \quad (6)$$

but ft values are usually large, so they are normally expressed in term of "log ft" values [20]. The log ft value is defined as

$$\log ft = \log_{10}(f_0 t_{1/2}[\text{s}]). \quad (7)$$

The shape factor $C(w_e)$ in Eq. (5) for pure Gamow-Teller transition is defined as

$$C(w_e) = \frac{g_A^2}{2J_i + 1}|\mathcal{M}_{\rm GT}|^2, \quad (8)$$

where the J_i is the angular momentum of the initial state, g_A is the axial-vector coupling constant, and the $\mathcal{M}_{\rm GT}$ is the Gamow-Teller nuclear matrix element [20], which is defined as

$$\mathcal{M}_{\rm GT} \equiv (\xi_f J_f \| \sigma \| \xi_i J_i) = \sum_{pn} \mathcal{M}_{\rm GT}(pn)(\xi_f J_f \| [c_p^\dagger \tilde{c}_n]_1 \| \xi_i J_i), \quad (9)$$

where $\mathcal{M}_{\rm GT}(pn)$ are the single-particle matrix elements (SPMEs). In case of forbidden nonunique β decay, the form of the shape factor $C(w_e)$ in Eq. (5) is defined as

$$C(w_e) = \sum_{k_e, k_\nu, K} \lambda_{k_e} \Big[M_K(k_e, k_\nu)^2 + m_K(k_e, k_\nu)^2 - \frac{2\gamma_{k_e}}{k_e w_e} M_K(k_e, k_\nu) m_K(k_e, k_\nu) \Big], \quad (10)$$

where the indices k_e and k_ν ($k_e, k_\nu = 1, 2, 3, \ldots$) are positive integers, which are emerging from the partial-wave expansion of the lepton wave functions and K is the order of forbiddenness of the transition. The nuclear structure information is contained in the quantities $M_K(k_e, k_\nu)$ and $m_K(k_e, k_\nu)$, which are complicated combinations of different nuclear matrix elements (NMEs) and leptonic phase-space factors. The factor λ_{k_e} is the Coulomb function and is expressed as

$$\lambda_{k_e} = \frac{F_{k_e - 1}(Z, w_e)}{F_0(Z, w_e)}, \quad (11)$$

where $F_{k_e-1}(Z, w_e)$ is the generalized Fermi function [9,18], which is expressed as

$$F_{k_e-1}(Z, w_e) = 4^{k_e - 1}(2k_e)(k_e + \gamma_{k_e})[(2k_e - 1)!!]^2 e^{\pi y} \times \left(\frac{2p_e R}{\hbar}\right)^{2(\gamma_{k_e} - k_e)} \left(\frac{|\Gamma(\gamma_{k_e} + iy)|}{\Gamma(1 + 2\gamma_{k_e})}\right)^2. \quad (12)$$

The auxiliary quantities are defined as $\gamma_{k_e} = [k_e^2 - (\alpha Z)^2]^{1/2}$ and $y = (\alpha Z w_e/p_e c)$, where $\alpha = 1/137$ is the fine structure constant.

The nuclear matrix elements (NMEs) are given by

$$^{V/A}\mathcal{M}_{KLS}^{(N)}(pn)(k_e, m, n, \rho) = \frac{1}{\sqrt{2J_i + 1}} \sum_{pn} {}^{V/A}m_{KLS}^{(N)}(pn)(k_e, m, n, \rho)(\psi_f \| [c_p^\dagger \tilde{c}_n] \| \psi_i). \quad (13)$$

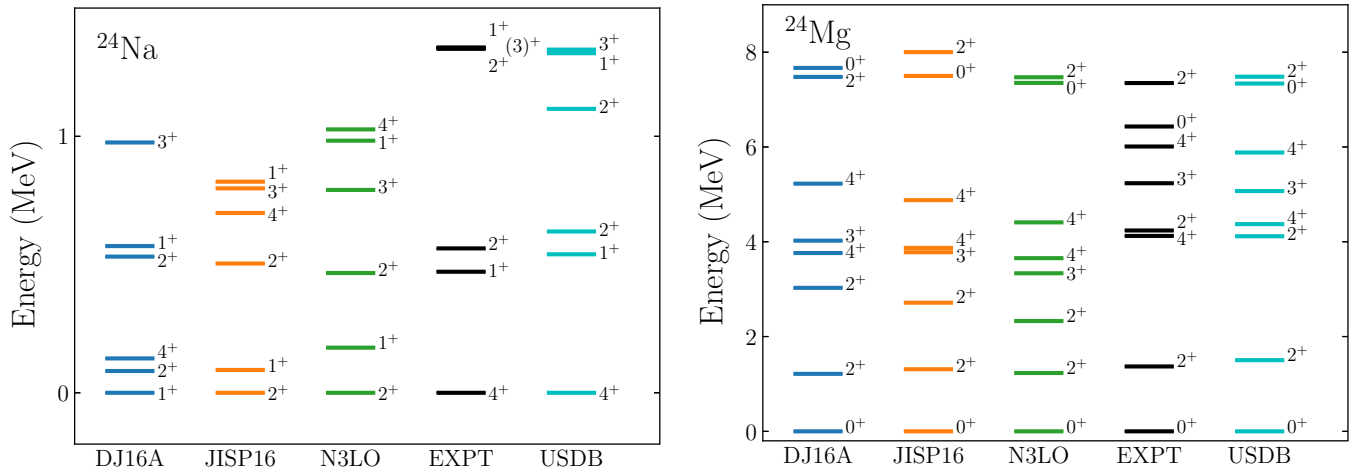

FIG. 1. Comparison of calculated and experimental [15] low-lying energy spectra for positive parity states of ^{24}Na and ^{24}Mg from microscopic and USDB interactions.

The nuclear matrix elements are divided in two parts: the first part ${}^{V/A}m^{(N)}_{KLS}(pn)(k_e, m, n, \rho)$ is called the single-particle matrix element and the second part $(\psi_f \| [c^\dagger_p \tilde{c}_n] \| \psi_i)$ is the reduced one-body transition density (OBTD) between the initial (i) and final (f) nuclear states. The single-particle matrix elements characterize the properties of the transition operators, so they are the same for all nuclear models. But the OBTDs are nuclear model dependent. In the present work the SPMEs are calculated using harmonic-oscillator wave functions (see Refs. [9,18]). The summation of Eq. (13) runs over the proton (p) and neutron (n) single-particle states.

The shape factor $C(w_e)$ (10) can be decomposed into vector, axial-vector, and mixed vector–axial-vector components [8,9,21–23] in the form

$$C(w_e) = g_V^2 C_V(w_e) + g_A^2 C_A(w_e) + g_V g_A C_{VA}(w_e). \quad (14)$$

After the integration of Eq. (14) with respect to electron kinetic energy, we get an expression analogous to Eq. (5) for the integrated shape function $\tilde{C}$:

$$\tilde{C} = g_V^2 \tilde{C}_V + g_A^2 \tilde{C}_A + g_V g_A \tilde{C}_{VA}. \quad (15)$$

In Eq. (14) the shape factors C_i are functions of the electron kinetic energy, while the integrated shape factors $\tilde{C}_i$ in Eq. (15) are just constant numbers.

B. ADOPTED MODEL SPACE AND HAMILTONIANS

In the present work shell model calculations for the low-lying energy spectra, log ft values, shape factors, and electron spectra of the β^- decay branches of ^{24}Na and ^{36}Cl were performed in the *sd* model space. In this framework we have calculated the OBTDs related to the NMEs of the shape factor. For the *sd* model space, we have used the three microscopic effective interactions DJ16A [24], JISP16 [25], and N3LO [25]. These interactions are obtained from the no-core shell model (NCSM) wave functions via the Okubo-Lee-Suzuki (OLS) unitary transformation [26–28]. We have also compared our results with the phenomenological USDB effective interaction [29]. The interaction "DJ16" [24] is obtained from the Daejeon16 NN potential [30]. After the monopole modification of DJ16, the interaction is labeled as "DJ16A" [24]. In this work, we have used the DJ16A interaction for further calculations. The OBTDs for NMEs were computed by the shell model code NuShellX [31]. For the evaluation of the many-body matrix elements, we have used the single-particle matrix element expression given in Ref. [16]. In our shell model calculations, we have used the single-particle matrix elements in the Condon-Shortley [32] phase convention.

III. RESULTS AND DISCUSSION

In this section we present our calculated results of low-lying energy spectra, nuclear matrix elements, log ft values, shape factors, electron spectra, and decomposition of the integrated shape factors for the second-forbidden nonunique β^- transitions of ^{24}Na$(4^+) \rightarrow {}^{24}Mg(2^+)$ and ^{36}Cl$(2^+) \rightarrow {}^{36}Ar(0^+)$.

Previously, the log ft values and shape factors of the second-forbidden β decay of ^{36}Cl [14] have been reported by applying two different nuclear models: with pure $1d_{3/2} \rightarrow 1d_{3/2}$ transitions and using the shell model with *sd* shell configuration space.

Recently, much progress has been achieved in developing modern effective interactions for the shell model calculations. Thus we have revisited the calculation for ^{36}Cl and also for the first time for ^{24}Na with recently developed microscopic (DJ16A, N3LO, and JISP16) and phenomenological (USDB) interactions in the *sd* model space. Our results for ^{24}Na will be useful when compared with upcoming experimental data.

Below we have presented low-lying energy spectra (Figs. 1 and 2), nuclear matrix elements (Tables I and III), log ft values (Table II and IV), shape factors, and electron spectra (Figs. 3 and 4). The low-lying energy spectra are discussed in Sec. III A. The β decay nuclear matrix elements and log ft values are discussed in Sec. III B. Results of the shape factors and electron spectra are presented in Sec. III C. Decomposition of the integrated shape factor are discussed in Sec. III D.

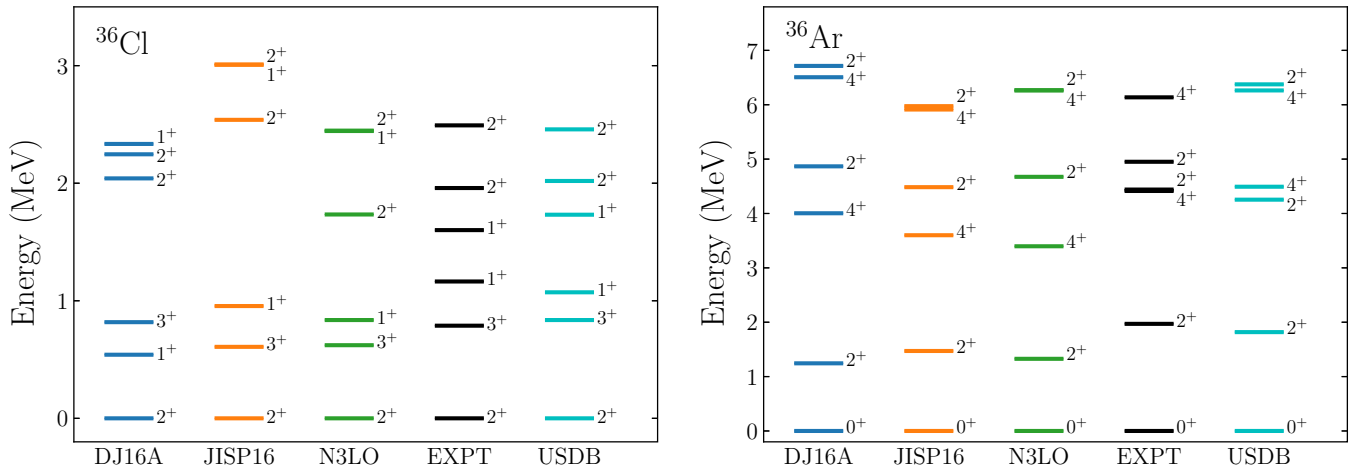

FIG. 2. Comparison of calculated and experimental [15] low-lying energy spectra for positive parity states of ^{36}Cl and ^{36}Ar from microscopic and USDB interactions.

A. Low-lying energy spectra

In Fig. 1, we show the low-lying energy spectra of ^{24}Na and ^{24}Mg. In the case of ^{24}Na, the ground state (g.s.) 4^+ is correctly reproduced by USDB interaction, while the other microscopic effective interactions N3LO and JISP16 give 2^+ as a g.s., and DJ16A predicts the g.s. as 1^+. The low-energy spectrum of the well known *sd*-shell rotor nucleus ^{24}Mg is already shown in Ref. [24] for all the interactions that we have used in the present work. For ^{24}Mg, the $0^+_{g.s.}$ and 2^+_1 are relatively well described by all the interactions. The computed 2^+_1 state is obtained at 1.213, 1.310, 1.231, and 1.502 MeV corresponding to DJ16A, JISP16, N3LO, and USDB, respectively, while the corresponding experimental value is 1.369 MeV. The theoretical low-lying energy spectra of ^{36}Cl and ^{36}Ar are shown in Fig. 2 in comparison with the experimental data. The g.s. is correctly reproduced by the microscopic (DJ16A, JISP16, and N3LO) and USDB interactions for ^{36}Cl and ^{36}Ar. For ^{36}Cl, the order of 3^+_1 and 1^+_1 states is correctly reproduced from the JISP16, N3LO, and USDB interactions as in the experimental data, while the DJ16A interaction inverts the order of these states. In the case of ^{36}Ar, the calculated 2^+_1 state values from the DJ16A, JISP16, N3LO, and USDB interactions are close to the experimental data. So, in general, the comparison of the computed low-lying energy levels shows good agreement with the experimental data for ^{24}Na, ^{36}Cl, and ^{36}Ar. In the present work we have taken Q values from the experimental data [15] for further calculations listed in Tables II and IV.

TABLE I. Calculated Gamow-Teller matrix elements of the allowed β^- decays from the g.s. (4^+) of ^{24}Na to the excited states in ^{24}Mg from microscopic and USDB effective interactions.

	$\lvert\mathcal{M}_{\rm GT}\rvert$				
Transitions	USDB	DJ16A	N3LO	JISP16	Expt.
$4^+ \to 3^+_1$	0.1859	0.1982	0.2274	0.2108	0.1179
$4^+ \to 4^+_1$	0.2663	0.0441	0.1069	0.0839	0.2072

B. Nuclear matrix elements and log ft values

The nuclear matrix elements contain the nuclear-structure information. The Gamow-Teller matrix elements $\mathcal{M}_{\rm GT}$ calculated from the microscopic and USDB interactions for the allowed β^- decays of ^{24}Na(4^+) $\to$ ^{24}Mg($3^+_1, 4^+_1$) transitions are presented in Table I with comparison to the experimental data. The experimental $\mathcal{M}_{\rm GT}$ value is obtained from the log ft [15] values corresponding to the axial-vector coupling constant $g_A = 1.00$. In the present work, we have calculated these matrix elements by using OBTDs corresponding to all microscopic and USDB interactions. After that, we compare the calculated $\mathcal{M}_{\rm GT}$ with the experimental data. For both allowed transitions, the calculated $\mathcal{M}_{\rm GT}$ values from USDB are close to the experimental data as compared to the microscopic interactions. In the case of the ^{24}Na(4^+) $\to$ ^{24}Mg(4^+_1) transition, our calculated value of $\mathcal{M}_{\rm GT}$ (0.0441) from DJ16A is very small in comparison with the experimental data.

The calculated log ft values of allowed β^- decays of ^{24}Na(4^+) $\to$ ^{24}Mg($3^+_1, 4^+_1$) transitions are presented in Table II in comparison to the experimental data. For the calculation, we have used the axial-vector coupling constants $g_A = 1.00$ and $g_A = 1.27$. For the transition $4^+ \to 3^+_1$, the calculated log ft values for $g_A = 1.00$ are in nice agreement with the experimental values corresponding to USDB, also all other microscopic effective interactions are in a reasonable agreement. However, in the case of the $4^+ \to 4^+_1$ transition, the calculated log ft value from DJ16A is larger in comparison with the experimental data, but those from other interactions are close to the experimental data with both g_A values.

For the second-forbidden nonunique β^- decays of ^{24}Na(4^+) $\to$ ^{24}Mg(2^+) and ^{36}Cl(2^+) $\to$ ^{36}Ar(0^+), the computed NMEs from different microscopic and USDB effective interactions are presented in Table III. The relativistic matrix element $^{V}\mathcal{M}^{(0)}_{211}$ is becoming identically zero due to the limitation of our $0\hbar\omega$ *sd*-shell calculations for harmonic-oscillator wave functions. To get the value of the $^{V}\mathcal{M}^{(0)}_{211}$ matrix element nonzero we need to perform shell model calculations in the multi-$\hbar\omega$ excitations. However, here we

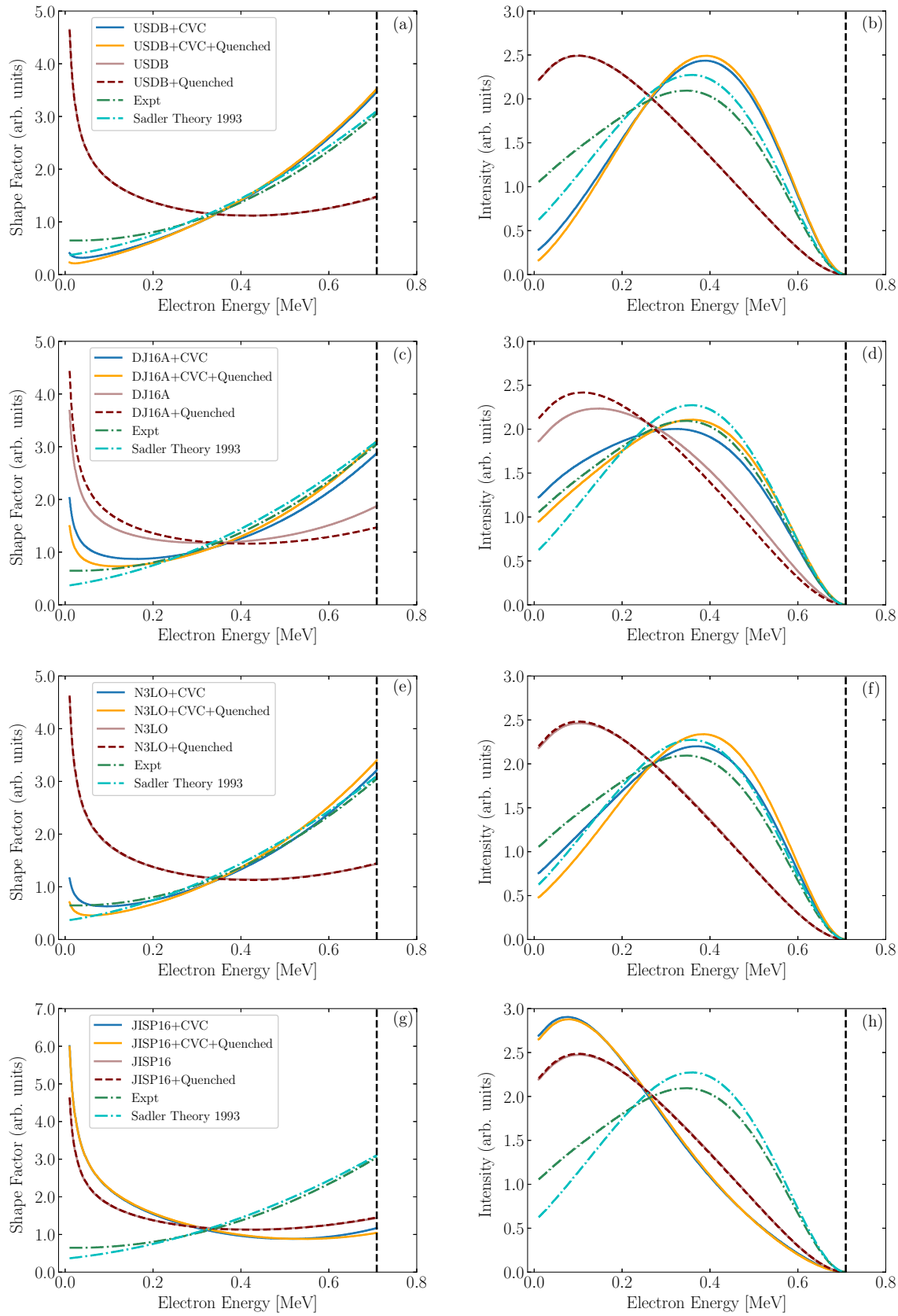

FIG. 3. Theoretical shape factors (left panels) and electron spectra (right panels) for second-forbidden β^- decay of $^{36}\mathrm{Cl}(2^+) \rightarrow {}^{36}\mathrm{Ar}(0^+)$ as functions of electron kinetic energy for different cases. The dashed vertical lines indicate the end-point energy for forbidden ($Q_{\mathrm{forbidden}}$) decay. The areas under each curve is normalized to unity.

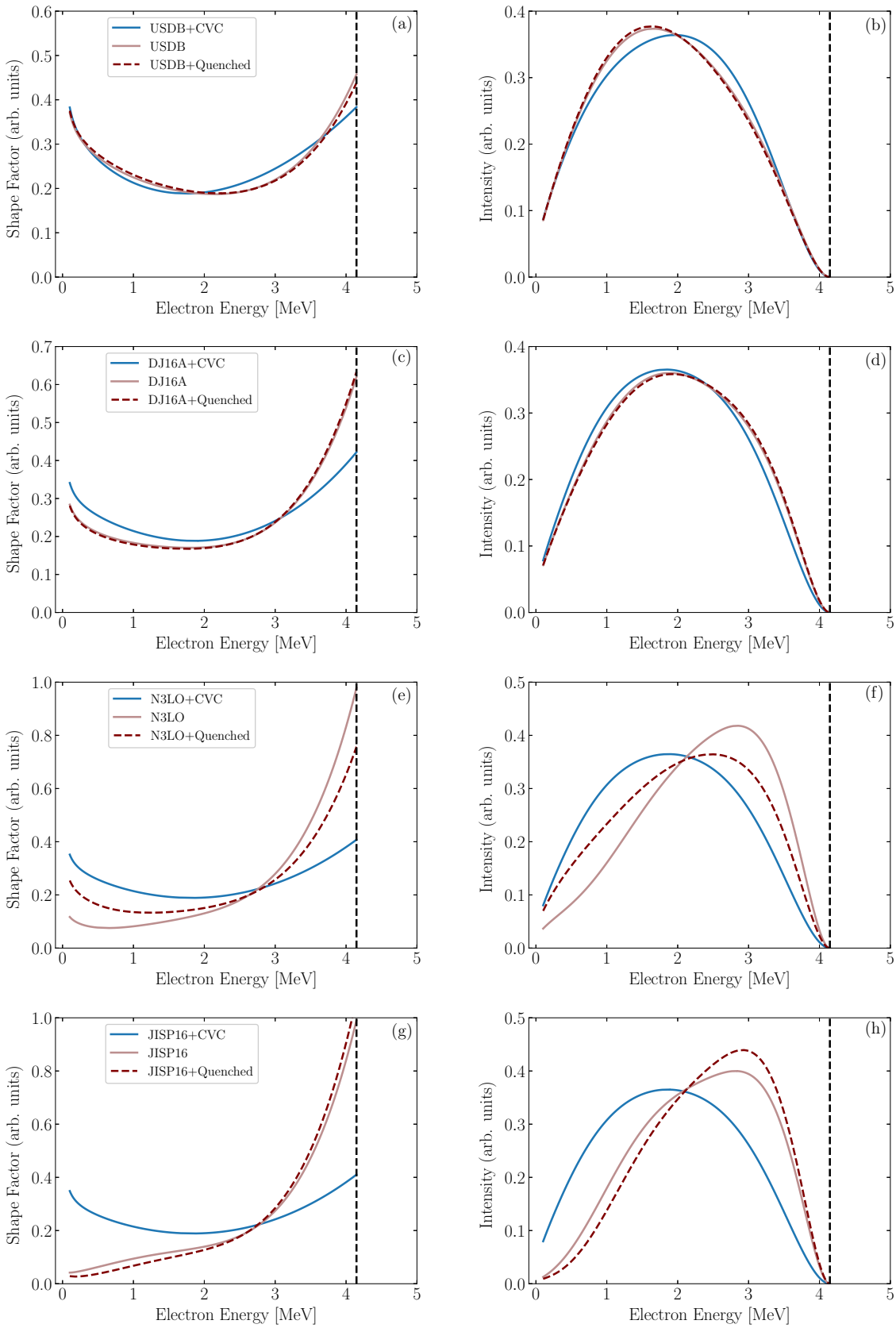

FIG. 4. Theoretical shape factors (left panels) and electron spectra (right panels) for second-forbidden β^- decay of $^{24}\mathrm{Na}(4^+) \rightarrow {}^{24}\mathrm{Mg}(2^+)$ as functions of electron kinetic energy for different cases. The dashed vertical lines indicate the end-point energy for forbidden ($Q_{\mathrm{forbidden}}$) decay. The area under each curve is normalized to unity.

TABLE II. Calculated log ft values of the allowed β^- decays from g.s. (4^+) of ^{24}Na to the excited states in ^{24}Mg from the microscopic and USDB effective interactions.

			log $ft(g_A = 1.00)$				log $ft(g_A = 1.27)$				
Transitions	Q (MeV)	BR (%)	USDB	DJ16A	N3LO	JISP16	USDB	DJ16A	N3LO	JISP16	Expt.
$4^+ \to 3^+_1$	0.280	0.076	6.205	6.149	6.029	6.095	5.997	5.941	5.822	5.888	6.60(2)
$4^+ \to 4^+_1$	1.392	99.855	5.892	7.454	6.685	6.896	5.685	7.247	6.478	6.688	6.11(1)

follow a different approach to calculate the $^V\mathcal{M}^{(0)}_{211}$ matrix element. We have used an approach based on CVC theory, since we have an experimental partial half-life, so we keep the value of coupling constants $g_V = g_A = 1.0$ and try to reproduce the value of the experimental partial half-life by varying the matrix element $^V\mathcal{M}^{(0)}_{211}$. The $^V\mathcal{M}^{(0)}_{211}$ matrix element obtained with this approach is labeled as "$^V\mathcal{M}^{(0)}_{211}$(CVC)" in Table III.

The axial-vector matrix elements $^A\mathcal{M}^{(0)}_{221}$, $^A\mathcal{M}^{(0)}_{221}(1,1,1,1)$, $^A\mathcal{M}^{(0)}_{221}(2,1,1,1)$, and $^A\mathcal{M}^{(0)}_{321}$ could be affected by the quenching of axial-vector coupling constant g_A. The affected value of the Gamow-Teller transition matrix element by the quenching of the axial coupling constant was observed in [33]. From a recent study of the second-forbidden nonunique β decay of ^{20}F, the effect of the quenching of the axial-vector coupling constant in axial-vector matrix elements is reported in Refs. [3,4]. Here, we will use the value of the axial-vector coupling constant for the two different cases: either the bare value of $g_A = 1.27$ or the quenched value of $g_A = 1.00$.

In Table IV, we presented the log ft values for the second-forbidden nonunique β^- decays of ^{24}Na and ^{36}Cl calculated with different microscopic and phenomenological interactions in comparison with the experimental data, and the values of coupling constants are taken as $g_A = 1.27$ and $g_V = 1.00$ for the calculations. The results with the pure shell model are labeled as "SM," and those constrained by experimental information are labeled as "SM + CVC." The prediction of log ft values with SM is far from the experimental data. However, the agreement between the calculation with "SM+CVC" and the experimental value came out to be very satisfactory.

C. Shape factors and electron spectra

In Figs. 3 and 4, we have shown the shape factors (left panels) and β spectra (right panels) of the second forbidden

TABLE III. Calculated leading-order nuclear matrix elements (NMEs) of the second-forbidden nonunique β^- decays of ^{24}Na and ^{36}Cl are from microscopic and USDB interactions. The Coulomb-corrected NMEs are indicated by (k_e, m, n, ρ), when such elements exist.

Nuclear matrix elements	^{24}Na(4^+) $\to$ ^{24}Mg(2^+)			
	USDB	DJ16A	N3LO	JISP16
$^V\mathcal{M}^{(0)}_{211}$(CVC)	0.023790±0.0001	−0.018446±0.0002	−0.020217±0.0001	−0.019636±0.0001
$^V\mathcal{M}^{(0)}_{220}$	0.431273	−0.131891	−0.237936	−0.187614
$^V\mathcal{M}^{(0)}_{220}(1,1,1,1)$	0.530979	−0.123441	−0.264185	−0.203108
$^V\mathcal{M}^{(0)}_{220}(2,1,1,1)$	0.509588	−0.110404	−0.247587	−0.189152
$^A\mathcal{M}^{(0)}_{221}$	−0.430287	−0.482638	−0.219655	−0.294803
$^A\mathcal{M}^{(0)}_{221}(1,1,1,1)$	−0.524687	−0.577264	−0.287289	−0.370261
$^A\mathcal{M}^{(0)}_{221}(2,1,1,1)$	−0.502493	−0.550486	−0.279212	−0.356859
$^A\mathcal{M}^{(0)}_{321}$	−1.459626	−0.758772	−0.067127	−0.050213
Nuclear matrix elements	^{36}Cl(2^+) $\to$ ^{36}Ar(0^+)			
	USDB	DJ16A	N3LO	JISP16
$^V\mathcal{M}^{(0)}_{211}$(CVC)	−0.029375±0.0005	−0.015943±0.0010	−0.022497±0.0008	−0.007451±0.0009
$^V\mathcal{M}^{(0)}_{220}$	−5.892542	−3.483430	−4.705624	−5.057782
$^V\mathcal{M}^{(0)}_{220}(1,1,1,1)$	−7.250832	−4.357072	−5.796787	−6.225284
$^V\mathcal{M}^{(0)}_{220}(2,1,1,1)$	−6.955989	−4.195245	−5.562475	−5.972497
$^A\mathcal{M}^{(0)}_{221}$	−1.249043	−2.025348	−1.716437	−1.644994
$^A\mathcal{M}^{(0)}_{221}(1,1,1,1)$	−1.496326	−2.412741	−2.062063	−1.979877
$^A\mathcal{M}^{(0)}_{221}(2,1,1,1)$	−1.426626	−2.297321	−1.967308	−1.889710

TABLE IV. Calculated $\log ft$ values of the second-forbidden nonunique β^- decays of ^{24}Na and ^{36}Cl from the shell model and after constraining the matrix element $^{V}\mathcal{M}^{(0)}_{211}$ from experimental data. For the $\log ft$ calculations we have used the values of coupling constants $g_V = 1.00$ and $g_A = 1.27$. The experimental data have been taken from [15].

				$\log ft$(SM)				
Transitions	Type	Q (MeV)	BR (%)	USDB	DJ16A	N3LO	JISP16	Expt.
^{24}Na(4^+) → ^{24}Mg(2^+)	2nd nonunique forbidden	4.147	0.064	12.237	12.881	14.227	13.958	11.340(4)
^{36}Cl(2^+) → ^{36}Ar(0^+)	2nd nonunique forbidden	0.710	98.1	12.635	13.978	13.120	12.976	13.321(3)
				$\log ft$(SM+CVC)				
Transitions	Type	Q (MeV)	BR (%)	USDB	DJ16A	N3LO	JISP16	Expt.
^{24}Na(4^+) → ^{24}Mg(2^+)	2nd nonunique forbidden	4.147	0.064	11.367	11.331	11.346	11.342	11.340(4)
^{36}Cl(2^+) → ^{36}Ar(0^+)	2nd nonunique forbidden	0.710	98.1	13.221	13.108	13.153	13.555	13.321(3)

nonunique β^- decays of ^{36}Cl and ^{24}Na. The second-forbidden nonunique β decay of ^{36}Cl is predicted with a strong branching ratio of 98.1%, while that of ^{24}Na is predicted with a weak branching ratio less than 1%. These figures represent the shape factor of Eq. (10) and β spectrum corresponding to the integrand of Eq. (5) as a function of electron kinetic energy for different microscopic and USDB effective interactions. For all these calculations of second-forbidden nonunique β decay of ^{24}Na and ^{36}Cl, we have used the experimentally measured Q values 4147 and 709.547 keV, respectively. We have calculated the shape factor by including only the leading-order terms, and the value of vector coupling constant $g_V = 1.00$ was adopted from the CVC hypothesis. We present in the figures the purely theoretical results from the shell model interactions, labeled with the name of the interaction, and those constrained from experimental information labeled with the name of the interaction and "+CVC," for quenched ($g_A = 1.00$) and bare ($g_A = 1.27$) cases. The areas under both

TABLE V. The dimensionless integrated shape factors $\tilde{C}$ for the studied transitions, and their decompositions to vector $\tilde{C}_V$, axial-vector $\tilde{C}_A$, and vector–axial-vector $\tilde{C}_{VA}$ parts. For the calculation of total integrated shape factor $\tilde{C}$ we have taken $g_V = g_A = 1.0$.

	^{24}Na(4^+) → ^{24}Mg(2^+)(SM)			
Interactions	$\tilde{C}_V$	$\tilde{C}_A$	$\tilde{C}_{VA}$	$\tilde{C}$
USDB	1.3982×10^{-6}	3.6829×10^{-6}	1.7841×10^{-6}	6.8653×10^{-6}
DJ16A	9.8078×10^{-8}	1.6952×10^{-6}	-5.1005×10^{-7}	1.2833×10^{-6}
N3LO	3.7996×10^{-7}	2.2572×10^{-7}	-5.0839×10^{-7}	9.7291×10^{-8}
JISP16	2.2998×10^{-7}	3.7051×10^{-7}	-5.0759×10^{-7}	9.2903×10^{-8}
	^{24}Na(4^+) → ^{24}Mg(2^+)(SM+CVC)			
Interactions	$\tilde{C}_V$	$\tilde{C}_A$	$\tilde{C}_{VA}$	$\tilde{C}$
USDB	8.3097×10^{-5}	3.6829×10^{-6}	-1.3924×10^{-5}	7.2856×10^{-5}
DJ16A	5.8298×10^{-5}	1.6952×10^{-6}	1.2868×10^{-5}	7.2861×10^{-5}
N3LO	6.5792×10^{-5}	2.2572×10^{-7}	6.8432×10^{-6}	7.2861×10^{-5}
JISP16	6.3828×10^{-5}	3.7051×10^{-7}	8.6647×10^{-6}	7.2864×10^{-5}
	^{36}Cl(2^+) → ^{36}Ar(0^+)(SM)			
Interactions	$\tilde{C}_V$	$\tilde{C}_A$	$\tilde{C}_{VA}$	$\tilde{C}$
USDB	6.0691×10^{-9}	3.1198×10^{-10}	-2.7292×10^{-9}	3.6519×10^{-9}
DJ16A	2.1890×10^{-9}	8.1048×10^{-10}	-2.6419×10^{-9}	3.5761×10^{-10}
N3LO	3.8787×10^{-9}	5.9273×10^{-10}	-3.0074×10^{-9}	1.4641×10^{-9}
JISP16	4.4736×10^{-9}	5.4657×10^{-10}	-3.1016×10^{-9}	1.9186×10^{-9}
	^{36}Cl(2^+) → ^{36}Ar(0^+)(SM+CVC)			
Interactions	$\tilde{C}_V$	$\tilde{C}_A$	$\tilde{C}_{VA}$	$\tilde{C}$
USDB	4.0126×10^{-10}	3.1198×10^{-10}	-7.7968×10^{-11}	6.3528×10^{-10}
DJ16A	1.4791×10^{-10}	8.1048×10^{-10}	-3.2311×10^{-10}	6.3528×10^{-10}
N3LO	2.5097×10^{-10}	5.9273×10^{-10}	-2.0843×10^{-10}	6.3527×10^{-10}
JISP16	2.2999×10^{-9}	5.4657×10^{-10}	-2.2112×10^{-9}	6.3528×10^{-10}

the theoretical and experimental curves are normalized to unity.

For the shape factor and β spectrum of ^{36}Cl, we have done a comparison with the available experimental data due to Rotzinger *et al.* [34] and with the theoretical results of Sadler *et al.* [14]. In the case of ^{36}Cl, the shape factor calculated with the matrix element ${}^{V}\mathcal{M}^{(0)}_{211} = 0$ yields a poor agreement in comparison to the experimental shape factor. After constraining this matrix element with the experimental half-life, the shape factor and electron spectra are consistent with the experimental data. The electron spectra from "DJ16A+CVC+Quenched" are perfectly matched with the experimental electron spectra. This means that the shape factor and electron spectra strongly depend on the matrix element ${}^{V}\mathcal{M}^{(0)}_{211}$. But in the case of the JISP16 interaction, we have not obtained a good number of this matrix element from the experimental half-life method. We have obtained the value of the matrix element ${}^{V}\mathcal{M}^{(0)}_{211} = -0.007451 \pm 0.0009$ for the JISP16 interaction; it is too small as compared to other interactions.

In Fig. 4, we have presented the shape factor and β spectrum of ^{24}Na from a pure shell model calculation with quenched and unquenched cases. In the pure shell model calculations, the shape-factor and β-spectrum curves depend strongly on the quenching value of g_A. After CVC constraining the matrix element ${}^{V}\mathcal{M}^{(0)}_{211}$, we find that the shape factor and β spectrum are independent of the value of g_A. So, we have presented the curve for "SM+CVC" only for the bare g_A value.

For comparison, there are no experimental data available for shape factor and electron spectra corresponding to the second-forbidden nonunique β^- decay of ^{24}Na. Thus, our theoretical results might be quite useful to compare with a future experimental measurement.

D. Decomposition of the integrated shape factor

In Table V, we present the integrated shape factor $\tilde{C}$ and its decomposition to vector $\tilde{C}_V$, axial-vector $\tilde{C}_A$, and mixed vector–axial-vector $\tilde{C}_{VA}$ components, for the involved transitions using different effective interactions. Hence, we have calculated the value of $\tilde{C}$ and its components with the pure shell model, labeled "SM," and after constraining the matrix element ${}^{V}\mathcal{M}^{(0)}_{211}$ from experimental information, labeled "SM+CVC." For all the studied decays transition, the sign of vector $\tilde{C}_V$ and axial-vector $\tilde{C}_A$ components is positive from SM and SM+CVC, but the sign of the mixed axial-vector $\tilde{C}_{VA}$ component varies. From the pure SM for ^{24}Na, the axial-vector component $\tilde{C}_A$ is dominant in the USDB and DJ16A interactions. For N3LO and JISP16 interactions, the mixed component $\tilde{C}_{VA}$ is roughly the sum of vector and axial-vector components and negative in sign. In SM+CVC, the vector component $\tilde{C}_V$ is dominant for all interactions. The mixed component $\tilde{C}_{VA}$ is negative for USDB, while positive for other interactions. In case of ^{36}Cl, the vector component $\tilde{C}_V$ is dominant for all the interactions in the case of the pure SM. After applying CVC theory, the vector part is dominant only in USDB and JISP16 interactions and for the other two interactions the axial-vector part is large as compared to the other two components. The signs of the mixed components $\tilde{C}_{VA}$ are negative in both cases SM and SM+CVC for all interactions.

IV. CONCLUSIONS

In this article we have calculated $\log ft$ values, shape factors, and electron spectra for the second-forbidden nonunique β^- transitions of $^{24}\mathrm{Na}(4^+) \rightarrow {}^{24}\mathrm{Mg}(2^+)$ and $^{36}\mathrm{Cl}(2^+) \rightarrow {}^{36}\mathrm{Ar}(0^+)$ using the three microscopic effective interactions (DJ16A, N3LO, and JISP16) obtained from the NCSM wave functions via the OLS transformation. Also, for comparison, we have used the more popular phenomenological effective USDB interaction.

The low-lying energy spectra of the involved mother and daughter nuclei in β^- decay corresponding to different *ab initio* and phenomenological effective interactions are compared with the available experimental data. The obtained wave functions have been used for further calculations. To calculate the $\log ft$ values, shape factors and electron spectra, we have constrained the relativistic matrix element ${}^{V}\mathcal{M}^{(0)}_{211}$ in the *sd* model space using experimental information. This matrix element plays an important role in the shape factors and electron spectra. The calculated $\log ft$ values are compared with experimental data. In the case of the JISP16 interaction, we could not obtain a proper value of this matrix element. In our calculation, we have used two different values of g_A, either the bare value of $g_A = 1.27$ or the quenched value of $g_A = 1.00$. For the allowed β decay of ^{24}Na, the $\log ft$ values are in reasonable agreement with the experimental data. In the case of second-forbidden nonunique β decay, we have calculated $\log ft$ values corresponding to $g_A = 1.27$ and compared them with the experimental data. Before applying CVC theory the electron spectra of ^{24}Na depend significantly on the effective value of g_A, while after applying CVC they have become independent. In the case of ^{36}Cl, the dependency of electron spectra on g_A is opposite from the case of ^{24}Na for USDB, N3LO, and JISP16 interactions, but in the case of the DJ16A interaction the electron spectra strongly depend on g_A before and after applying CVC theory. In the case of ^{36}Cl, the experimental data are available for shape factors and electron spectra. So we have compared our theoretical results with the experimental data to check the role of matrix element ${}^{V}\mathcal{M}^{(0)}_{211}$. But in the case of ^{24}Na, there are no experimental data available for shape factors and electron spectra. Thus, our calculated results could be quite useful for comparison with future experimental data. Also, we have decomposed the integrated shape function $\tilde{C}$ into vector $\tilde{C}_V$, axial-vector $\tilde{C}_A$, and vector–axial-vector $\tilde{C}_{VA}$ components to see the individual effects of these components.

ACKNOWLEDGMENTS

A.K. would like to thank the Ministry of Human Resource Development (MHRD), Government of India, for financial support for his thesis work. P.C.S. acknowledges a research grant from SERB (India), CRG/2019/000556. We would like to thank X. Mougeot for providing the experimental shape factor data of ^{36}Cl.

[1] K. Langanke and G. Martínez-Pinedo, Nuclear weak-interaction processes in stars, Rev. Mod. Phys. **75**, 819 (2003).

[2] B. Singh, J. Rodriguez, S. Wong, and J. Tuli, Review of logft values in β decay, Nucl. Data Sheets **84**, 487 (1998).

[3] O. S. Kirsebom *et al.*, Measurement of the $2^+ \rightarrow 0^+$ ground-state transition in the β decay of ^{20}F, Phys. Rev. C. **100**, 065805 (2019).

[4] O. S. Kirsebom *et al.*, Discovery of an Exceptionally Strong β-Decay Transition of ^{20}F and Implications for the Fate of Intermediate-Mass Stars, Phys. Rev. Lett. **123**, 262701 (2019).

[5] T. Suzuki, S. Zha, S.-C. Leung, and K. Nomoto, Electron-capture Rates in ^{20}Ne for a forbidden transition to the ground state of ^{20}F relevant to final evolution of high-density O-Ne-Mg cores, Astrophys. J. **881**, 64 (2019).

[6] H. Ejiri, J. Suhonen, and K. Zuber, Neutrino-nuclear responses for astro-neutrinos, single beta decays and double beta decays, Phys. Rep. **797**, 1 (2019).

[7] M. Haaranen, P. C. Srivastava, J. Suhonen, and K. Zuber, β decay half-life of ^{50}V calculated by the shell model, Phys. Rev. C **90**, 044314 (2014).

[8] M. Haaranen, P. C. Srivastava, and J. Suhonen, Forbidden nonunique β decays and effective values of weak coupling constants, Phys. Rev. C **93**, 034308 (2016).

[9] M. Haaranen, J. Kotila, and J. Suhonen, Spectrum-shape method and the next-to-leading-order terms of the β-decay shape factor, Phys. Rev. C **95**, 024327 (2017).

[10] A. Kumar, P. C. Srivastava, and T. Suzuki, Shell model results for nuclear β^--decay properties of sd-shell nuclei, Prog. Theor. Exp. Phys. **2020**, 033D01 (2020).

[11] V. Kumar, P. C. Srivastava, and H. Li, Nuclear β^--decay half-lives for fp and fpg shell nuclei, J. Phys. G: Nucl. Part. Phys. **43**, 105104 (2016).

[12] A. Saxena, P. C. Srivastava, and T. Suzuki, *Ab initio* calculations of Gamow-Teller strengths in the sd shell, Phys. Rev. C **97**, 024310 (2018).

[13] V. Kumar and P. C. Srivastava, Shell model description of Gamow-Teller strengths in pf-shell nuclei, Eur. Phys. J. A **52**, 181 (2016).

[14] R. Sadler and H. Behrens, Second-forbidden beta-decay and the effect of $(V + A)$- and S-interaction admixtures: ^{36}Cl, Z. Phys. A **346**, 25 (1993).

[15] National Nuclear Data Center (NNDC), ENSDF database, 2020, https://www.nndc.bnl.gov/ensdf/.

[16] H. Behrens and W. Bühring, *Electron Radial Wave Functions and Nuclear Beta-Decay* (Clarendon, Oxford, 1982).

[17] H. F. Schopper, *Weak Interaction and Nuclear Beta Decay* (North-Holland, Amsterdam, 1966).

[18] M. T. Mustonen, M. Aunola, and J. Suhonen, Theoretical description of the fourth-forbidden non-unique β decays of ^{113}Cd and ^{115}In, Phys. Rev. C **73**, 054301 (2006); **76**, 019901(E) (2007)

[19] E. Ydrefors, M. T. Mustonen, and J. Suhonen, MQPM desription of the structure and beta decays of the odd $A = 95, 97$ Mo and Tc isotopes, Nucl. Phys. A **842**, 33 (2010).

[20] J. Suhonen, *From Nucleons to Nucleus: Concept of Microscopic Nuclear Theory* (Springer, Berlin, 2007).

[21] J. Kostensalo, M. Haaranen, and J. Suhonen, Electron spectra in forbidden β decays and the quenching of the weak axial-vector coupling constant g_A, Phys. Rev. C **95**, 044313 (2017).

[22] J. Kostensalo and J. Suhonen, g_A-driven shapes of electron spectra of forbidden β decays in the nuclear shell model, Phys. Rev. C **96**, 024317 (2017).

[23] J. Suhonen, Value of the axial-vector coupling strength in β and $\beta\beta$ decays: A review, Front. Phys. **5**, 55 (2017).

[24] N. A. Smirnova, B. R. Barrett, Y. Kim, I. J. Shin, A. M. Shirokov, E. Dikmen, P. Maris, and J. P. Vary, Effective interactions in the sd shell, Phys. Rev. C **100**, 054329 (2019).

[25] E. Dikmen, A. F. Lisetskiy, B. R. Barrett, P. Maris, A. M. Shirokov, and J. P. Vary, *Ab initio* effective interactions for sd-shell valence nucleons, Phys. Rev. C **91**, 064301 (2015).

[26] S. Okubo, Diagonalization of Hamiltonian and Tamm-Dancoff equation, Prog. Theor. Phys. **12**, 603 (1954).

[27] K. Suzuki and S. Y. Lee, Convergent theory for effective interaction in nuclei, Prog. Theor. Phys. **64**, 2091 (1980).

[28] K. Suzuki, Construction of Hermitian effective interaction in nuclei: General relation between Hermitian and non-Hermitian forms, Prog. Theor. Phys. **68**, 246 (1982).

[29] B. A. Brown and W. A. Richter, New "USD" Hamiltonians for the sd shell, Phys. Rev. C **74**, 034315 (2006).

[30] A. M. Shirokov, I. J. Shin, Y. Kim, M. Sosonkina, P. Maris, and J. P. Vary, N3LO NN interaction adjusted to light nuclei in *ab exitu* approach, Phys. Lett. B **761**, 87 (2016).

[31] B. A. Brown and W. D. M. Rae, The shell-model code NuShellX@MSU, Nucl. Data Sheets **120**, 115 (2014).

[32] E. U. Condon and G. Shortley, *The Theroy of Atomic Spectra* (Cambridge University Press, Cambridge, 1951).

[33] I. S. Towner, Quenching of spin matrix elements in nuclei, Phys. Rep. **155**, 263 (1987).

[34] H. Rotzinger, M. Linck, A. Burck, M. Rodrigues, M. Loidl, E. Leblanc, L. Fleischmann, A. Fleischmann, and C. Enss, Beta spectrometry with magnetic calorimeters, J. Low. Temp. Phys. **151**, 1087 (2008).